PHOTONICS Research

Principles to tailor the saturable and reverse saturable absorption of epsilon-near-zero material

Hao Ma,[1,2,3] Yuanan Zhao,[1,2,3,*] Yuchen Shao,[1,2,3] Yafei Lian,[1,2,3] Weili Zhang,[1,2,3] Guohang Hu,[1,2,3] Yuxin Leng,[4] and Jianda Shao[1,2,3,5,6]

[1]Laboratory of Thin Film Optics, Shanghai Institute of Optics and Fine Mechanics, Chinese Academy of Sciences, Shanghai 201800, China
[2]Center of Materials Science and Optoelectronics Engineering, University of Chinese Academy of Sciences, Beijing 100049, China
[3]Key Laboratory of Materials for High Power Laser, Chinese Academy of Sciences, Shanghai 201800, China
[4]State Key Laboratory of High Field Laser Physics, Shanghai Institute of Optics and Fine Mechanics, Chinese Academy of Sciences, Shanghai 201800, China
[5]Hangzhou Institute for Advanced Study, University of Chinese Academy of Sciences, Hangzhou 310024, China
[6]e-mail: jdshao@siom.ac.cn
*Corresponding author: yazhao@siom.ac.cn

Received 15 December 2020; revised 27 February 2021; accepted 27 February 2021; posted 1 March 2021 (Doc. ID 417642); published 15 April 2021

Indium tin oxide (ITO) films have recently emerged as a new class of functional materials for nonlinear optical (NLO) devices due to their exotic properties around epsilon-near-zero (ENZ) wavelength. Here, we experimentally investigated and tailored the NLO absorption properties of ITO films. The NLO absorption response of ITO films is investigated by using the femtosecond Z-scan measurement technique at two different wavelengths of 1030 nm (out of ENZ region) and 1440 nm (within ENZ region). Interestingly, we observed conversion behavior from saturable absorption (SA) to reverse saturable absorption (RSA) at 1030 nm with the increasing incident laser intensity, whereas only SA behavior was observed at 1440 nm. We demonstrate that SA behavior was ascribed to ground-state free electrons bleaching in the conduction band, and RSA was attributed to three-photon absorption. Moreover, results reveal that ITO film shows more excellent SA performance at 1440 nm with a nonlinear absorption coefficient of ~ -23.2 cm/GW and a figure of merit of $\sim 1.22 \times 10^{-16}$ esu · cm. Furthermore, we tailored the SA and RSA behaviors of ITO films at 1030 and 1440 nm wavelengths via post-annealing treatment. The modulatable NLO absorption was ascribed to the changing of free-carrier concentration in ITO films via annealing treatment. The experimental findings offered an inroad for researchers to tailor its NLO absorption properties by changing the free-carrier concentration through chemical modification such as annealing, oxidation, or defect implantation. The superior and tunable nonlinear optical response suggests that ITO film might be employed as a new class material with potential applications in novel optical switches or optical limiters to realize the all-optical information process.

https://doi.org/10.1364/PRJ.417642

1. INTRODUCTION

Transparent conductive oxides (TCOs) that function as thin films exhibit high electrical conductivity and good transparency in the visible range [1,2]. Owing to the unique characteristics of TCOs with electrical conductivity, high optical transmittance, and wide bandgap (3.2–4.2 eV), they are widely applied in electronics and optoelectronics applications [3–6]. In recent studies, TCOs exhibit interesting nonlinear optical (NLO) responses over a wide spectral region (from visible to midinfrared), especially in the epsilon-near-zero (ENZ) region [7–10], where the real and imaginary parts of dielectric constant simultaneously approach zero for materials. A vanishing dielectric permittivity leads to the large optical nonlinearity due to the enhanced nonlinear refractive index and the local field effect when approaching the ENZ wavelength [11,12]. Indium tin oxide (ITO) thin film is one of the most commonly used TCOs, for which the ENZ wavelength is located in the near-infrared range. As a heavily doped oxide semiconductor, it has been proven that its ENZ wavelength and dielectric properties can be tailored by changing the free-carrier concentration via doping or post-annealing treatment [13–17]. Recently, lots of fantastic NLO effects of ITO film, including nonlinear absorption [18–20], Kerr nonlinearity [12,21–23], and four-wave mixing [24], have been exploited. Among them, nonlinear absorption effects [e.g., saturable absorption (SA) or reverse saturable absorption (RSA)] are always one of the most compelling and intensive research topics. The SA effect is usually used to

generate short laser pulses by Q-switching or passive mode-locking techniques [25–28]. The RSA effect can be useful for applications in optical limiters to protect eyes or sensors [25,26]. The SA and SA responses involve the high-intensity light field and are dependent on the intrinsic properties of optical materials. The enhancement of electric fields in the ENZ region should be favorable for the generation of SA or RSA effects. However, SA and RSA effects are two competing nonlinear responses, which are affected by the wavelength or intensity of the incident radiation [29,30]. Recently, quite a few investigations into SA and RSA effects of the ITO film or other refractory materials like TiN have been conducted [31–34]. For example, Ali *et al.* observed that, under the excitation wavelength from 720 to 900 nm, the nonlinear absorption coefficient of ITO film depended on the wavelength and input intensity, but the nonlinear refractive only was wavelength dependent [31]. Elin *et al.* observed the optical Kerr nonlinearity and its carrier concentration dependence in ITO films with femtosecond laser pulses at 780 nm [34]. In addition, Kinsey *et al.* and George *et al.* investigated the nonlinearities and carrier dynamics in TiN thin film by using dual Z-scan and nondegenerate transient pump-probe techniques [32,33]. Past research has not focused on intrinsic competitive mechanism of the NLO absorption in ITO film. Moreover, intrinsic competitive mechanisms and the tailoring of this competition remain largely unexplored. Therefore, an in-depth investigation of the aforementioned competitive mechanism can enable us to further understand the inherent optical properties of ITO film and then promote additional applications of ITO film in the field of optoelectronics.

In this paper, we prepared ITO films using an electron beam evaporation method and chose two different wavelengths of 1030 nm (out of ENZ region) and 1440 nm (within ENZ region) to analyze the electron transition behavior related to SA and RSA. Our results show conversion behavior from SA to RSA at 1030 nm with increasing incident laser intensity, whereas only SA behavior was observed at 1440 nm. We found that ground-state free electrons bleaching in the conduction band and three-photon absorption play a vital role in this conversion. In the SA process, a large nonlinear absorption coefficient $\beta \sim -23.2$ cm/GW and a figure of merit of $\sim 1.22 \times 10^{-16}$ esu · cm were obtained at 1440 nm. Furthermore, we tailored the free-carrier concentration by post-annealing treatment to obtain adjustable dielectric properties and analyzed the electron absorption behavior of the annealed ITO film. Results reveal that the NLO absorption response behavior and response amplitude of ITO film can be tailored via post-annealing treatment. By analyzing and tailoring the NLO properties of ITO films, we can design films with low saturable intensity or large three-photon absorption coefficient, thereby enabling their potential application in ultrafast lasers or optical limiting devices.

2. EXPERIMENTS

A. ITO Film Preparation

In this work, ITO films were deposited on fused-silica substrates (10 mm × 10 mm × 1 mm) using the electron beam evaporation technique with a baking temperature of 200°C and base pressure lower than $\sim 2 \times 10^{-3}$ Pa. Before deposition, the substrates were ultrasonically cleaned in acetone, ethanol, and deionized water for 30 min and subsequently dried with a flow of nitrogen. The film thickness was 200 nm with 10% Sn-doping. The evaporation rate and thickness were monitored by a quartz crystal (SQM-160). All substrates were placed on the fixture at the same radius from the axis to ensure uniform film thickness. Post-annealing treatments were carried out using a high-temperature tubular furnace. The ITO films annealing in air atmosphere were maintained for 2 h at 400°C.

B. Characterization of ITO Films

The surface morphologies of the as-deposited and annealed ITO films were examined by scanning electron microscopy (SEM). The SEM images in Figs. 1(a) and 1(b) show a regular surface with small-sized uniformly distributed particles in both as-deposited and annealed ITO films. The structure properties and the crystalline quality of the films were evaluated by a Bruker AXS/D8 Advance X-ray diffraction (XRD) system (Bruker, Billerica, MA, USA) with Cu Kα radiation ($\lambda = 0.15408$ nm). Figure 1(c) presents the XRD patterns in the scan range of 10°–70° for the as-deposited and annealed ITO films. XRD patterns of the ITO films showed peaks in orientations of (211), (222), (400), (440), and (622), suggesting a polycrystalline with cubic bixbyite In_2O_3 structure. The intensity of (222) peak was slightly enhanced after the annealing process, implying that the crystallinity of the films was enhanced. The linear optical transmittance was measured with a UV/VIS/NIR spectrometer (Lambda 1050, Perkins Elmer, Waltham, MA, USA) over the spectral range of 200–1800 nm, as shown in Fig. 1(d). Typically, transmittance improvement in the visible region after annealing is ascribed to the enhanced crystallinity, which subsequently reduces grain-boundary scattering [35]. The small crystallinity improvement observed before and after annealing in our experiments was consistent with the insignificant change in transmittance in the visible region. However, in the near-IR region, the free-carrier absorption becomes important for the transmittance of the ITO films [35,36]. From Fig. 1(d), we can see that, in the near-infrared range, the transmittance of the ITO films increased after annealing process, which is due to the decrease of free electrons in the ITO film due to annealing in the air.

C. Determination of ENZ Wavelength of ITO Films

To locate the ENZ region of the as-deposited and annealed ITO films, the optical properties of the ITO films were characterized by spectroscopic ellipsometry (HORIBA, UVISEL 2 series, Japan) in the spectral region from 400 to 2000 nm. The dielectric function of the ITO film can be well described using the Drude–Lorentz oscillator model [37]. In ITO film, conduction band electrons have a near continuum of available states, so the conduction band electrons can be treated as a 3D free-electrons gas if we ignore the nonlocal effects. The interaction with an electromagnetic field is described by the Drude model. The Lorentz oscillator model is used to describe the absorption of photons by valence band electrons. According to the Drude–Lorentz oscillator model, the permittivity of ITO film is given by

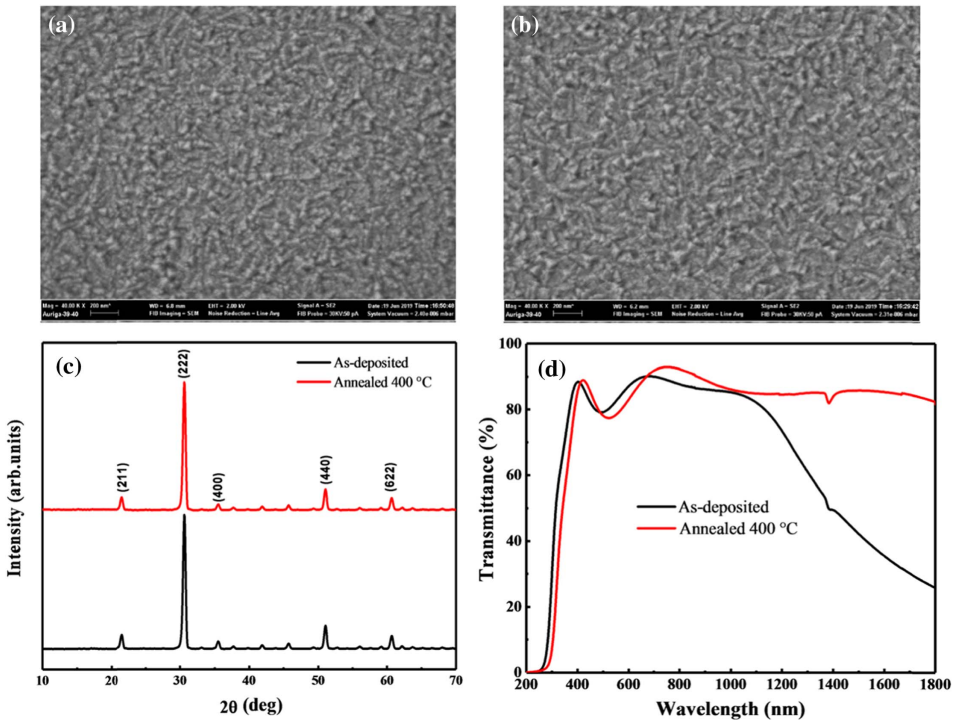

Fig. 1. Characterization of as-deposited and annealed ITO films. SEM images showing (a) as-deposited ITO film and (b) ITO film annealed at 400°C. (c) X-ray diffraction pattern. (d) Linear optical transmittance spectrum.

$$\varepsilon(\omega) = 1 - \frac{\omega_{p,b}^2}{\omega^2 - \omega_{0,b}^2 + i\gamma_b\omega} - \frac{\omega_p^2}{\omega^2 + i\gamma_f\omega}. \quad (1)$$

In this model, $\omega_p = (Ne^2/\varepsilon_0 m^*)^{1/2}$ is the unscreened plasma frequency, where N is the free-electron density, e is the electronic charge, m^* is the effective free electron mass, γ_f is the free-electron damping coefficient, $\omega_{p,b}$ is the bound electron plasma frequency, $\omega_{0,b}$ is the resonance frequency, and γ_b is the bound electron damping coefficient. The results are shown in Fig. 2. Notably, the ENZ point of the as-deposited ITO film is located at ~1.46 μm, whereas the ENZ point of the post-annealed ITO film is located at ~2.0 μm. The redshift of the ENZ point in the post-annealed ITO film is due to the decrease of the free-carrier concentration caused by annealing treatment [15,16,38,39].

D. Z-Scan Measurements

Nonlinear optical properties of the ITO films were investigated at 1030 and 1440 nm wavelengths using the femtosecond Z-scan technique developed by Sheik–Bahae [40]. The normalized open aperture (OA) transmittance provides information about the nonlinear absorption, while the normalized closed aperture (CA) transmittance merely represents the nonlinear refraction effect. The schematic of this optical setup is shown in Fig. 3. The films were excited by a fiber laser (1030 nm) and a commercial tunable femtosecond laser (1440 nm) with ~340 and ~45 fs pulse widths, respectively, both operating at 1 kHz repetition. Based on the related theory and research [41,42], the repetition rate of the pulsed laser in our Z-scan system is lower than the threshold that produces the thermal lens effect. The sample was mounted on a computer-controlled

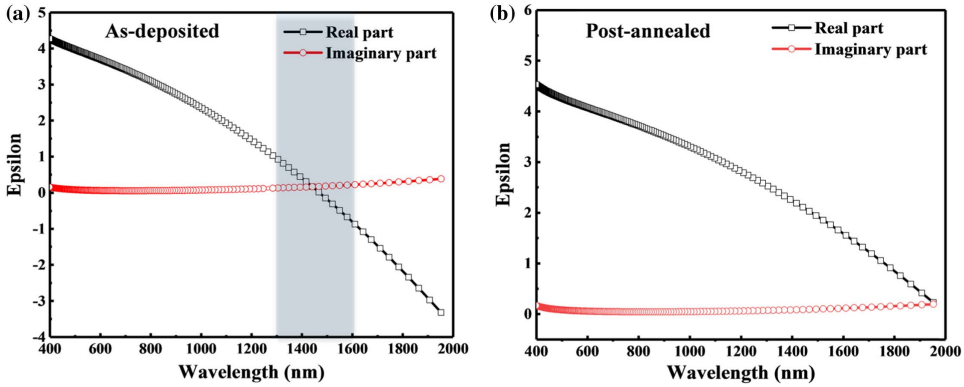

Fig. 2. Real and imaginary components of the permittivity of ITO films. (a) As-deposited ITO film. (b) Post-annealed ITO film.

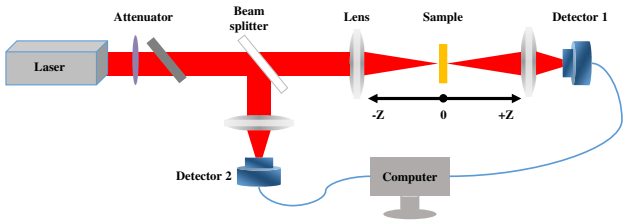

Fig. 3. Optical nonlinear absorption measurement setup based on the Z-scan method.

platform moving along the propagation direction of the laser beam (Z axis). A lens of 150 mm focal length focused the 1030 and 1440 nm laser beams on the sample to spots with radii of approximately 17 and 30 μm, respectively. A beam splitter divided the output laser beam into a signal and a reference parts, collected by detectors 1 and 2. A half-wave plate and a polarizer placed in the front of the lens are used to attenuate the beam intensity.

3. RESULTS AND DISCUSSION

A. Nonlinear Optical Absorption Properties of As-deposited ITO Films at 1030 nm

In Fig. 4(a), a typical OA Z-scan analysis of an ITO film, measured with 1030 nm laser excitation is shown, which was investigated at input intensities of 15.3, 24.5, 30.6, 45.9, and 61.2 GW/cm^2 (the fluence at focusing point). The nonlinear absorption (NLA) response of the ITO film revealed that the transmittance changed in a nonlinear manner with the incident pump intensity. First, we found the typical SA features, where the transmittance increases as the sample is moving to the beam waist ($Z = 0$), i.e., the incident light intensity increases, forming a transmission peak at the waist [29,30]. As the laser excitation intersity at the focal point increases, the SA modulation amplitude will further increase, whereas when the laser intensity at the focal plane increased approximately 91.8 GW/cm^2, a depletion cure appeared as shown in Fig. 4(b), which illustrated the phenomenon of the RSA effect [29,30]. Note that the transmittance curve exhibits a symmetrical valley with two humps, indicating the coexistence of SA and RSA effects [30]. Moreover, no signal was detected from blank quartz under the maximum achievable photo-excitation, confirming that only the ITO films contribute to the NLO response we measured. These results verify the strong nonlinear optical response and optical signal modulating capabilities of ITO films.

Generally speaking, for ITO film, the nonlinearities can be differentiated into two classes, depending on the relative energies of the bandgap and the optical pump. When an ultrafast optical pulse with energy smaller than the bandgap excites ITO films, the free electrons in the conduction band undergo intraband transitions via free-carrier absorption. However, when the incident fluence is high enough, the interband transitions may occur related to multiphoton absorption. Before excitation, the free electrons in the conduction band are in equilibrium and can be described by a room-temperature Fermi distribution. When the laser pulses excite ITO film, the electrons are energized, and their distribution is highly nonthermal, which produces a redshift of the plasma frequency. We can describe the optical response by means of a phenomenological two-temperature model [43,44]. For optical pulse energies greater than the bandgap or if the excitation intensity is strong enough, the interband transitions occur. The interband transitions increase the total free electron concentration, which causes the blueshift of plasma frequency. In addition, it is worth noting that the nonlocal effects play an important role in the nonlinearity of ultrathin films supporting ENZ and Berreman modes. Hydrodynamic models that account for both nonlinear and nonlocal contributions have been used to explain the nonlinearities and blueshift the plasma frequency of ENZ nanofilms such as ITO and doped-cadmium-oxide films (~20 nm thickness) [37,45,46]. The blueshift of the plasma frequency caused by nonlocal effects will in turn modify the absorption, which can change the free electron effective mass, causing the redshift of the plasma frequency. Therefore, the nonlocal effects and modulation of the plasma frequency are dynamic. The redshift of the plasma frequency tends to reduce the reflectivity, as the ITO film appears more dielectric, whereas the blueshift of the plasma frequency tends to increase the reflection, as the ITO film appears more metallic. Taking into account that the nonlinearities of free electrons, the third-order hot electron effect, and the high-order nonlocal effects may be competitive, if the third-order hot electron effect is dominant, the nonlinear response of ITO film exhibits an increase in transmittance (SA effect). The high-order nonlocal effect dominates the

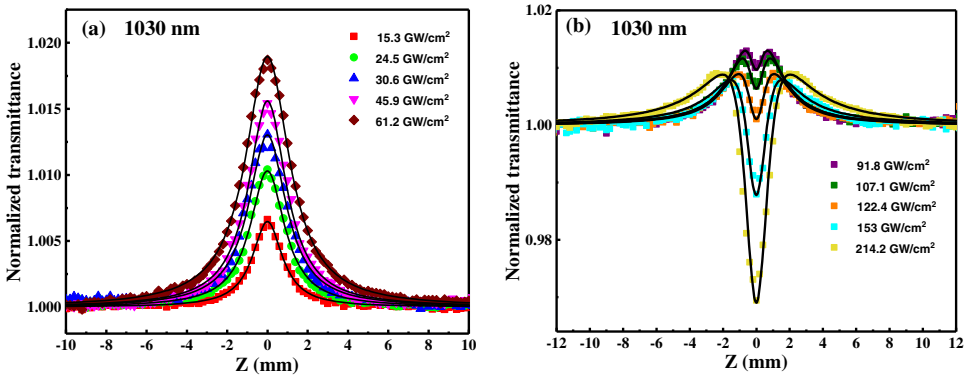

Fig. 4. Open aperture Z-scan results of as-deposited ITO films under excitation of 1030 nm at different input fluences.

Table 1. Saturated Absorption Intensity (I_s) and Corresponding Three-Photon Absorption Coefficient (γ)

Laser Intensity (GW/cm^2)	24.5	61.2	91.8	122.4	214.2
I_s (GW/cm^2)	64.4	67.1	76.1	105.9	88.5
γ (cm^3/GW^2)	3.6×10^{-3}	6.0×10^{-3}	4.9×10^{-2}	6.1×10^{-2}	8.8×10^{-2}

nonlinear response of the ITO film, which exhibits a decrease in transmittance (RSA effect). In our experiments, the thickness of all ITO films is 200 nm, so the nonlocal effects may be not obvious. Moreover, all Z-scan experiments were carried out at normal angle of incidence, so it is difficult to form ENZ or Berreman modes. Considering these, the most likely nonlinear response mechanisms in our experiments are dominated by intraband and interband transitions.

The observed SA behavior of ITO films can be attributed to the ground-state free electrons bleaching in the conduction band with anharmonic motion under a strong electromagnetic field excitation (intraband transitions) [22,47]. When the sample moves near the focal point, the enhanced electronmagnetic field inside the sample resonates with the incident light wave, which leads to absorption saturation and the increase of transmittance. With further increase in the laser excitation intensity, the RSA effect was observed, indicating another nonlinear process occurs. It is worth noting that, in the present experiments, the laser photon energy is 1.2 eV (1030 nm) and the bandgap of the ITO film was about 3.3–3.4 eV in our experiment, which satisfies $2h\nu < E_g < 3h\nu$. Therefore, the RSA effect may be related to three-photon absorption, which involves the bound electrons in the valence band transition to the conduction band by absorbing three photons simultaneously (interband transitions). For further verifying our speculations, we first analyze the absorption coefficient, which consists of the SA coefficient and the three-photon absorption coefficient, which is written as [30]

$$\alpha(I) = \frac{\alpha_0}{1 + I/I_s} + \gamma I^2, \tag{2}$$

where $\alpha(I)$ is the total absorption coefficient. The first term describes the SA (negative nonlinear aborption) and the second term describes the RSA (positive nonlinear absorption). α_0 and γ are the linear and nonlinear absorption coefficients, respectively; I and I_s are the incident laser and saturated absorption intensity, respectively. Based on the nonlinear optical theory, the light attenuation during propagating through an optical material can be expressed as

$$\frac{\mathrm{d}I}{\mathrm{d}z} = -\alpha(I)I. \tag{3}$$

Here, z is the propagating distance in the samples. Theoretical fit of the experimental data could be conducted by substituting Eq. (2) into Eq. (3). I_s and γ can be obtained by fitting the Z-scan curves, and the results are listed in Table 1. Solid lines in Figs. 4(a) and 4(b) show the theoretical fitting at different laser excitation intensities, which are in good agreement with the experimental results, indicating the model used is reasonable.

From Table 1, it is interesting to note that I_s and γ are dependent on the peak intensity at the focal point. The saturated absorption intensity increased monotonously when the laser intensity increased from 24.5 to 122.4 GW/cm^2 and then decreased with further intensity increase. In contrast, the three-photon absorption coefficient γ increased monotonically with increasing laser intensity over the whole interval measured. This change indicates competition between SA and RSA effects in the ITO films excited with 1030 nm light. At low incident intensity (61.2 GW/cm^2), the SA parameter I_s was the prominent factor; therefore, only SA behavior was detected. The three-photon absorption coefficient γ becomes significant when the laser intensity increased past 61.2 GW/cm^2, leading to the occurrence of the RSA effect. These changes show the competition between the ground-state free-electron bleaching and three-photon absorption.

B. Nonlinear Optical Properties of As-deposited ITO Films at 1440 nm

Figures 5(a) and 5(b) show the experimental curves of Z-scan for the as-deposited ITO films under 1440 nm excitation with OA and CA configurations, respectively. In contrast with the results obtained from 1030 nm excitation, only the SA response was observed under 1440 nm excitation, as shown in Fig. 5(a). Obviously, the photon energy corresponding to 1440 nm is ~0.86 eV, which is much smaller than the bandgap of ITO film (3.3–3.4 eV); therefore, the multiphoton absorption process is almost impossible, and the SA response is dominant. The experimental data in Fig. 5(a) can be fit by the traditional Z-scan model [40]:

$$T(z) = \sum_{m=0}^{\infty} \frac{[-q_0(z,0)]^m}{(m+1)^{3/2}}, \qquad q_0(z,0) = \frac{\beta L_{\mathrm{eff}} I_0}{1 + z^2/z_0^2}, \tag{4}$$

where $L_{\mathrm{eff}} = [1 - \exp(-\alpha_0 L)]/\alpha_0$ is the effective interaction length, α_0 is the linear absorption coefficient, β is the NLA coefficient, I_0 is the on-axis peak intensity at the focal plane, L is the sample thickness, and z_0 is the Rayleigh diffraction length.

To determine the sign and magnitude of the nonlinear refractive index of the as-deposited ITO films, a CA Z-scan measurement was subsequently conducted. The typical shape of the nonlinear refractive index can be extracted from the division of the CA measurement by the OA measurement. The CA/OA curves shown in Fig. 5(b) present a valley peak shape, which means a self-focusing behavior under the illumination of fs laser pulses, indicating a positive value of n_2. As for the CA Z-scan measurements, we fit the experimental data with the following function [40]:

$$T(z) = 1 - \frac{4\Delta\phi_0(z/z_0)}{(1 + z^2/z_0^2) + (9 + z^2/z_0^2)}, \tag{5}$$

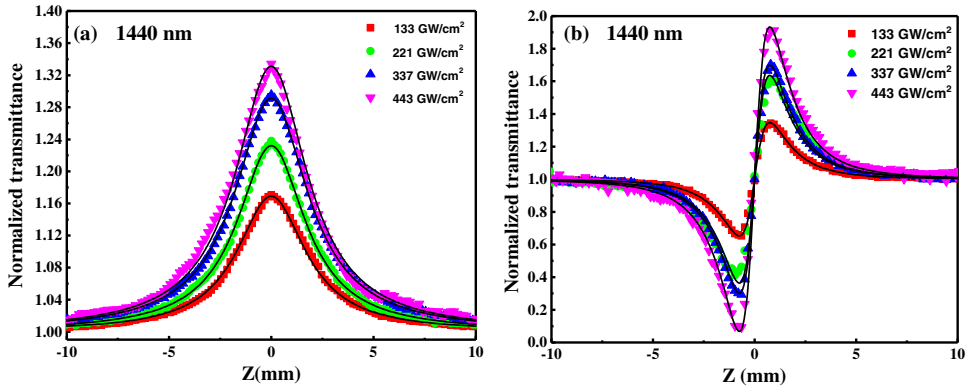

Fig. 5. Open aperture Z-scan results of as-deposited ITO films under excitation of 1440 nm at different input fluences. (a) OA Z-scan. (b) CA Z-scan.

where $\Delta\phi_0 = kn_2I_0L_{\text{eff}}$ is the on-axis phase change of the laser beam due to nonlinear refraction, $k = 2\pi/\lambda$ is the wavelength number, I_0 is the incident intensity at the focus point, L_{eff} is the effective interaction length, z is the longitudinal distance moved by the sample from the focus ($z = 0$), and z_0 is the Rayleigh diffraction length. The fitting results show that β and n_2 are as high as ~ -23.2 cm/GW and 1.02×10^{-3} cm^2/GW, respectively at 133 GW/cm^2. In addition, we evaluate the NLO performance of the ITO film. The imaginary part of the third-order NLO susceptibility is defined as follows [48–50]:

$$\text{Im}\chi^{(3)} = \frac{4}{3}n_0'\varepsilon_0 c\left(n_0'\beta\frac{\lambda}{4\pi} + n_0''n_2\right). \quad (6)$$

Here, ε_0 is the free space permittivity, c is the speed of light, λ is the wavelength, and other parameters are defined as follows. $\tilde{n} = \tilde{n_0} + \tilde{n_2}I$ is the total complex refractive index, including third-order nonlinearities; $\tilde{n_0} = n_0' + in_0''$ is the complex linear refractive index; $\tilde{n_2} = n_2' + in_2''$ is the complex nonlinear refractive index. The figure of merit (FOM) for the third-order optical nonlinearity is defined as FOM $= |\text{Im}\chi^{(3)}/\alpha_0|$, which can be used to eliminate the discrepancy caused by linear absorption. Therefore, Im$\chi^{(3)}$ and FOM for the ITO film under the excitation of 1440 nm are calculated as $\sim -1.60 \times 10^{-12}$ esu and $\sim 1.22 \times 10^{-16}$ esu · cm, respectively, where α_0 is $\sim 1.3027 \times 10^4$ cm^{-1}. The value of the FOM for ITO film is comparable with some other SA nanomaterials, such as MoS_2 ($\sim 1.47 \times 10^{-15}$ esu · cm) [51], graphene oxide ($\sim 4.2 \times 10^{-15}$ esu · cm) [52], and graphene ($\sim 5 \times 10^{-15}$ esu · cm) [52]. It can be inferred that the ITO film has a large SA response at 1440 nm, which suggests that this material might have potential for Q-switching, pulse compression, and mode locking in the near-infrared region.

C. Tailoring SA and RSA by Thermal Annealing

To further explore the characteristics of electronic nonlinear absorption in the ITO films, we changed the free-carrier concentration in the ITO films via post-annealing treatment. The NLA properties of the ITO films before and after annealing were tested under the same laser excitation conditions (at 1030 and 1440 nm). The intensity-dependent normalized transmittance of the ITO films (as-deposited and annealed) is shown in Figs. 6(a) and 6(b), respectively.

Obviously, as mentioned, for the as-deposited ITO film, the SA transforms into RSA upon increasing the excitation intensities at 1030 nm wavelength. The different NLA manifestations suggest that ITO film cannot only act as an optical switch at low incident intensity but also have potential applications as an optical limiter at high incident intensities. However, it is a consistent SA response under the excitation at 1440 nm wavelength. Interestingly, it can be seen from Fig. 6 that, compared with the excitation at 1030 nm, the SA effect of the as-deposited ITO film is more pronounced

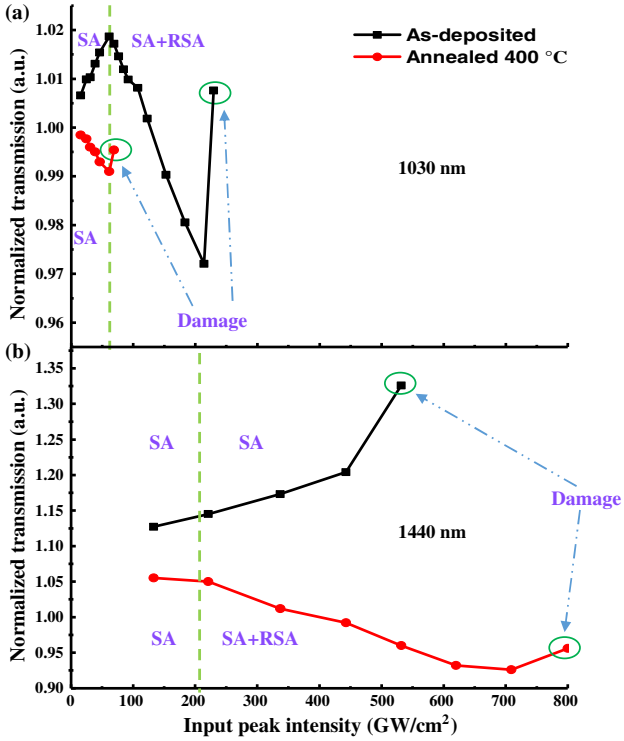

Fig. 6. Dependence of normalized transmittance of ITO films (as-deposited and annealed) on optical intensity using different pump sources. (a) 1030 nm. (b) 1440 nm.

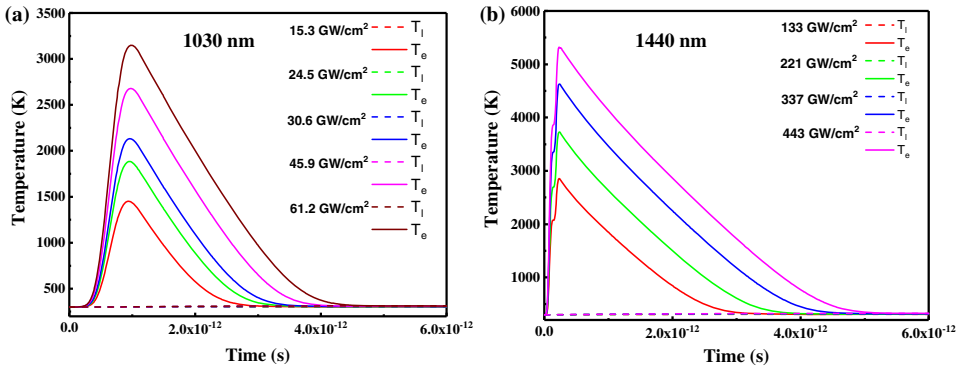

Fig. 7. Transient response of T_e and T_l obtained using the two-temperature model under different pump fluences. (a) 1030 nm excitation. (b) 1440 nm excitation.

under 1440 nm excitation. This phenomenon may come from the following two possibilities. One is that the large SA effect at 1440 nm (in ENZ region) is associated with the resonance absorption. If the pump frequency coincides with plasma frequency (at the zero-permittivity wavelength), the free electrons in the ITO film are excited resonantly [10,22]. In addition, under the excitation of 1030 nm wavelength, the SA and RSA are in a competitive relationship. Therefore, even at a small incident fluence, the RSA may still inhibit the SA. The observed nonlinearity is primarily due to a modification of the energy distribution of conduction-band electrons caused by laser-induced electron heating. We calculate the transient response of T_e (electron temperature) and T_l (lattice temperature) under 1030 and 1440 nm wavelength excitation at different incident fluence by using a two-temperature model. The results are shown in Fig. 7. It is worth noting that increasing the incident fluence causes the higher temperature of the hot electrons in the conduction band and the longer time for hot electrons and lattice to reach thermal equilibrium. Comparing Figs. 7(a) and 7(b), the temperature profile exhibits the one feature present in our experiment results shown in Fig. 6, namely, a pronounced enhancement SA effect of the response at 1440 nm wavelength. This provides guidance for us to apply ITO films as an optical switch, that is to say, we can design an optical switch with better SA effect by matching the ENZ wavelength to the optical switch wavelength. Moreover, through annealing treatment, we can tailor the NLA behavior of ITO films. As shown in Fig. 6(a), the annealed ITO film always shows RSA behavior when the input intensities vary from 15.3 to 61.2 GW/cm^2, whereas the as-deposited ITO film exhibits the SA effect. When the excitation intensity further increases, the as-deposited ITO film begins to exhibit the RSA effect, while damage occurs in the annealed ITO film. We observe that the minimum normalized transmittances are 0.991 and 0.972 for ITO films before and after annealing, respectively, indicating that the RSA effect of the annealed ITO film is suppressed. Additionally, the as-deposited ITO film exhibits damage behavior until the excitation intensity is 229.5 GW/cm^2, which is much higher than the annealed ITO film. In Fig. 6(b), the as-deposited film always behaves as the SA, whereas the annealed ITO film only exhibits the SA under low excitation intensity (133 GW/cm^2). Furthermore, under the excitation intensity of 443 GW/cm^2, the as-deposited ITO film shows the maximum normalized transmittance of 1.204, but the normalized transmittance of annealed ITO film is 0.99, indicating that annealing treatment can change the switching effect of ITO film in the near-IR region. For a better interpretation of this nonlinear optical absorption tailoring, the Hall effect properties of the samples were characterized by a four-probe method. The results are listed in Table 2. After the annealing treatment, the electrical properties of the ITO film were modified. The free-carrier concentration decreases to 1.6×10^{21} cm^{-3}, while the mobility increases to 39.7 cm^2/(V · s) for the annealed ITO film. Figure 6 shows that the SA effect of the annealed ITO film is suppressed under both wavelengths' excitation. After the annealing treatment, the free-carrier concentration in the conduction band of ITO film is reduced, which leads to suppression of ground-state free-electrons bleaching. Such dependence has been observed in semiconductors such as Si and Ge [53]. According to the free-electron theory [53], the SA coefficient (relating to the imaginary part of third-order susceptibility) is proportional to the free-carrier concentration. Consequently, we observed that the SA of annealed ITO film decreases, whereas the RSA related to the three-photon absorption increases.

Another interesting phenomenon is that the effect of annealing treatment on the resistance of ITO film to laser damage at the two wavelengths is opposite. Obviously, in Fig. 6(a) the damage threshold of the annealed ITO film is reduced when irradiated by the 1030 nm light. In contrast with the results obtained for 1030 nm light excitation, the annealed ITO offers better resistance to laser damage (532 GW/cm^2 for the as-deposited and 800 GW/cm^2 for the annealed ITO film, respectively) under the excitation of 1440 nm.

Table 2. Hall-Effect Properties of As-deposited and Annealed ITO Films

Samples	Carrier Concentration (cm^{-3})	Mobility [cm^2/(V · s)]	Resistivity (Ω · cm)
As-deposited	7.5×10^{21}	31.5	2.2
Annealed	1.6×10^{21}	39.7	11.9

This interesting phenomenon may originate from the fact that the ability of ITO film to resist laser damage depends on the competition between interband transitions and intraband transitions. Under 1030 nm laser irradiation, compared with the annealed ITO film, the conduction band of the deposited ITO film can be filled to a higher energy state due to the high free-carrier concentration, which leads to the suppression of interband transition. Therefore, the damage threshold of the annealed ITO film is reduced. However, under 1440 nm laser irradiation, the as-deposited ITO film has a lot of free electrons in the conduction band; therefore, the damage behavior is dominated by intraband transition. After annealing treatment, the free electron concentration is reduced, leading to the domination of interband transition. The results show that, by changing the free-carrier concentration in ITO film, we can design optical switching or an optical limiter with larger laser damage resistance at different wavelengths.

4. CONCLUSION

In summary, we systematically investigated the intrinsic mechanisms of NLO absorption in ITO films using the femtosecond Z-scan technique. The results reported in this work indicate that ITO films can exhibit switching between the SA and RSA response, depending on the irradiation wavelength and excitation intensity. Numerical fitting of the experimental data indicates that ground-state free electrons bleaching (third-order nonlinearity) and three-photon absorption (fifth-order nonlinearity) play a significant role in this conversion. The analysis, based on the nonlinear optical absorption model, shows that, under the excitation of a 1440 nm wavelength (within ENZ region), ITO films possess saturable absorption with an imaginary part of the third-order NLO susceptibility of $\sim -1.60 \times 10^{-12}$ esu and the FOM of $\sim 1.22 \times 10^{-16}$ esu · cm. Moreover, we experimentally demonstrated that the NLA responses and the resistance to laser damage of ITO films can be tailored by annealing treatment. These changes are attributed to the change in free-electron concentration induced by annealing treatment. Investigating and tailoring the NLO responses of ITO films can drive the further development and applications for ITO films in the fields of optoelectronics and photonics.

Funding. National Natural Science Foundation of China (11874369, U1831211); Strategic Priority Research Program of the Chinese Academy of Sciences (XDB1603).

Disclosures. The authors declare no conflicts of interest.

REFERENCES

1. H. Wang, X. Jiao, Q. Liu, X. Xuan, F. Chen, and W. Wu, "Transparent and conductive oxide films of the perovskite $La_xSr_{1-x}SnO_3$ ($x \leq 0.15$): epitaxial growth and application for transparent heterostructures," J. Phys. D **43**, 035403 (2010).
2. J. F. Wager, "Transparent electronics," Science **300**, 1245–1246 (2003).
3. C. G. Granqvist and A. Hultaker, "Transparent and conducting ITO films: new developments and applications," Thin Solid Films **411**, 1–5 (2002).
4. H. Taha, K. Ibrahim, M. M. Rahman, D. J. Henry, C.-Y. Yin, J.-P. Veder, A. Amri, X. Zhao, and Z.-T. Jiang, "Sol-gel derived ITO-based bi-layer and tri-layer thin film coatings for organic solar cells applications," Appl. Surf. Sci. **530**, 147164 (2020).
5. X. Li, Z. Deng, J. Li, Y. Li, L. Guo, Y. Jiang, Z. Ma, L. Wang, C. Du, Y. Wang, Q. Meng, H. Jia, W. Wang, W. Liu, and H. Chen, "Hybrid nanoscale Au with ITO structure for a high-performance near-infrared silicon-based photodetector with ultralow dark current," Photon. Res. **8**, 1662–1670 (2020).
6. E. W. Li, B. A. Nia, B. K. Zhou, and A. X. Wang, "Transparent conductive oxide-gated silicon microring with extreme resonance wavelength tunability," Photon. Res. **7**, 473–477 (2019).
7. D. C. Adams, S. Inampudi, T. Ribaudo, D. Slocum, S. Vangala, N. A. Kuhta, W. D. Goodhue, V. A. Podolskiy, and D. Wasserman, "Funneling light through a subwavelength aperture with epsilon-near-zero materials," Phys. Rev. Lett. **107**, 133901 (2011).
8. Z. Wang, C. Chen, K. Wu, H. Chong, and H. Ye, "Transparent conductive oxides and their applications in near infrared plasmonics," Phys. Status Solidi A **216**, 1700794 (2019).
9. M. H. Javani and M. I. Stockman, "Real and imaginary properties of epsilon-near-zero materials," Phys. Rev. Lett. **117**, 107404 (2016).
10. E. G. Carnemolla, L. Caspani, C. DeVault, M. Clerici, S. Vezzoli, V. Bruno, V. M. Shalaev, D. Faccio, A. Boltasseva, and M. Ferrera, "Degenerate optical nonlinear enhancement in epsilon-near-zero transparent conducting oxides," Opt. Mater. Express **8**, 3392–3400 (2018).
11. M. Kamandi, C. Guclu, T. S. Luk, G. T. Wang, and F. Capolino, "Giant field enhancement in longitudinal epsilon-near-zero films," Phys. Rev. B **95**, 161105 (2017).
12. L. Caspani, R. P. Kaipurath, M. Clerici, M. Ferrera, T. Roger, J. Kim, N. Kinsey, M. Pietrzyk, A. Di Falco, V. M. Shalaev, A. Boltasseva, and D. Faccio, "Enhanced nonlinear refractive index in epsilon-near-zero materials," Phys. Rev. Lett. **116**, 233901 (2016).
13. N. Mitoma, S. Aikawa, W. Ou-Yang, X. Gao, T. Kizu, M.-F. Lin, A. Fujiwara, T. Nabatame, and K. Tsukagoshi, "Dopant selection for control of charge carrier density and mobility in amorphous indium oxide thin-film transistors: comparison between Si- and W-dopants," Appl. Phys. Lett. **106**, 042106 (2015).
14. O. Tuna, Y. Selamet, G. Aygun, and L. Ozyuzer, "High quality ITO thin films grown by dc and RF sputtering without oxygen," J. Phys. D **43**, 055402 (2010).
15. Y. Wang, A. Capretti, and L. Dal Negro, "Wide tuning of the optical and structural properties of alternative plasmonic materials," Opt. Mater. Express **5**, 2415–2430 (2015).
16. L. Peng, Y. A. Zhao, X. Liu, Z. Cao, D. Li, Y. Lian, Y. Cui, H. Ma, R. Hong, C. Tao, D. Zhang, and J. Shao, "Tailoring the free carrier and optoelectric properties of indium tin oxide film via quasi-continuous-wave laser annealing," Appl. Surf. Sci. **538**, 148104 (2021).
17. Q. Guo, Y. Cui, Y. Yao, Y. Ye, Y. Yang, X. Liu, S. Zhang, X. Liu, J. Qiu, and H. Hosono, "A solution-processed ultrafast optical switch based on a nanostructured epsilon-near-zero medium," Adv. Mater. **29**, 1700754 (2017).
18. J. Guo, H. N. Zhang, C. Zhang, Z. Li, Y. Q. Sheng, C. H. Li, X. H. Bao, B. Y. Man, Y. Jiao, and S. Z. Jiang, "Indium tin oxide nanocrystals as saturable absorbers for passively Q-switched erbium-doped fiber laser," Opt. Mater. Express **7**, 3494–3502 (2017).
19. Z. M. Zhang, J. J. Liu, Q. D. Hao, and J. Liu, "Sensitive saturable absorber and optical switch of epsilon-near-zero medium," Appl. Phys. Express **12**, 065504 (2019).
20. Q. H. Xiao, X. Y. Feng, W. Yang, Y. K. Lin, Q. Q. Peng, S. Z. Jiang, J. Liu, and L. B. Su, "Epsilon-near-zero indium tin oxide nanocolumns array as a saturable absorber for a Nd:BGO laser," Laser Phys. **30**, 055802 (2020).
21. P. Guo, R. D. Schaller, J. B. Ketterson, and R. P. H. Chang, "Ultrafast switching of tunable infrared plasmons in indium tin oxide nanorod arrays with large absolute amplitude," Nat. Photonics **10**, 267–273 (2016).
22. M. Z. Alam, I. De Leon, and R. W. Boyd, "Large optical nonlinearity of indium tin oxide in its epsilon-near-zero region," Science **352**, 795–797 (2016).

23. N. Kinsey, C. DeVault, J. Kim, M. Ferrera, V. M. Shalaev, and A. Boltasseva, "Epsilon-near-zero Al-doped ZnO for ultrafast switching at telecom wavelengths," Optica **2**, 616–622 (2015).
24. J. B. Khurgin, M. Clerici, V. Bruno, L. Caspani, C. DeVault, J. Kim, A. Shaltout, A. Boltasseva, V. M. Shalaev, M. Ferrera, D. Faccio, and N. Kinsey, "Adiabatic frequency shifting in epsilon-near-zero materials: the role of group velocity," Optica **7**, 226–231 (2020).
25. C. Lu, H. Xuan, Y. Zhou, X. Xu, Q. Zhao, and J. Bai, "Saturable and reverse saturable absorption in molybdenum disulfide dispersion and film by defect engineering," Photon. Res. **8**, 1512–1521 (2020).
26. J. Liu, H. Nie, B. Yan, K. Yang, H. Yang, V. Khayrudinov, H. Lipsanen, B. Zhang, and J. He, "Nonlinear optical absorption properties of InP nanowires and applications as a saturable absorber," Photon. Res. **8**, 1035–1041 (2020).
27. X. Feng, J. Liu, W. Yang, X. Yu, S. Jiang, T. Ning, and J. Liu, "Broadband indium tin oxide nanowire arrays as saturable absorbers for solid-state lasers," Opt. Express **28**, 1554–1560 (2020).
28. R. Wei, H. Zhang, X. Tian, T. Qiao, Z. Hu, Z. Chen, X. He, Y. Yu, and J. Qiu, "MoS_2 nanoflowers as high performance saturable absorbers for an all-fiber passively Q-switched erbium-doped fiber laser," Nanoscale **8**, 7704–7710 (2016).
29. C. Gu, H. Zhang, P. You, Q. Zhang, G. Luo, Q. Shen, Z. Wang, and J. Hu, "Giant and multistage nonlinear optical response in porphyrin-based surface-supported metal-organic framework nanofilms," Nano Lett. **19**, 9095–9101 (2019).
30. Y. Gao, X. Zhang, Y. Li, H. Liu, Y. Wang, Q. Chang, W. Jiao, and Y. Song, "Saturable absorption and reverse saturable absorption in platinum nanoparticles," Opt. Commun. **251**, 429–433 (2005).
31. M. Ali, A. Shehata, M. Ashour, W. Z. Tawfik, R. Schuch, and T. Mohamed, "Measuring the nonlinear optical properties of indium tin oxide thin film using femtosecond laser pulses," J. Opt. Soc. Am. B **37**, A139–A146 (2020).
32. H. George, J. Reed, M. Ferdinandus, C. DeVault, A. Lagutchev, A. Urbas, T. B. Norris, V. M. Shalaev, A. Boltasseva, and N. Kinsey, "Nonlinearities and carrier dynamics in refractory plasmonic TiN thin films," Opt. Mater. Express **9**, 3911–3924 (2019).
33. N. Kinsey, A. A. Syed, D. Courtwright, C. DeVault, C. E. Bonner, V. I. Gavrilenko, V. M. Shalaev, D. J. Hagan, E. W. Van Stryland, and A. Boltasseva, "Effective third-order nonlinearities in metallic refractory titanium nitride thin films," Opt. Mater. Express **5**, 2395–2403 (2015).
34. H. I. Elim, W. Ji, and F. Zhu, "Carrier concentration dependence of optical Kerr nonlinearity in indium tin oxide films," Appl. Phys. B **82**, 439–442 (2006).
35. J. H. Park, C. Buurma, S. Sivananthan, R. Kodama, W. Gao, and T. A. Gessert, "The effect of post-annealing on indium tin oxide thin films by magnetron sputtering method," Appl. Surf. Sci. **307**, 388–392 (2014).
36. T. A. Gessert, Y. Yoshida, C. C. Fesenmaier, and T. J. Coutts, "Sputtered In_2O_3 and ITO thin films containing zirconium," J. Appl. Phys. **105**, 083547 (2009).
37. L. Rodriguez-Sune, M. Scalora, A. S. Johnson, C. Cojocaru, N. Akozbek, Z. J. Coppens, D. Perez-Salinas, S. Wall, and J. Trull, "Study of second and third harmonic generation from an indium tin oxide nanolayer: influence of nonlocal effects and hot electrons," APL Photon. **5**, 010801 (2020).
38. Y. L. Hu, X. G. Diao, C. Wang, W. C. Hao, and T. M. Wang, "Effects of heat treatment on properties of ITO films prepared by rf magnetron sputtering," Vacuum **75**, 183–188 (2004).
39. P. F. Robusto and R. Braunstein, "Optical measurements of the surface-plasmon of indium tin oxide," Phys. Status Solidi A **119**, 155–168 (1990).
40. M. Sheikbahae, A. A. Said, T. H. Wei, D. J. Hagan, and E. W. Vanstryland, "Sensitive measurement of optical nonlinearities using a single beam," IEEE J. Quantum Electron. **26**, 760–769 (1990).
41. A. Gnoli, L. Razzari, and M. Righini, "Z-scan measurements using high repetition rate lasers: how to manage thermal effects," Opt. Express **13**, 7976–7981 (2005).
42. M. Falconieri, "Thermo-optical effects in Z-scan measurements using high-repetition-rate lasers," J. Opt. A **1**, 662–667 (1999).
43. M. Clerici, N. Kinsey, C. DeVault, J. Kim, E. G. Carnemolla, L. Caspani, A. Shaltout, D. Faccio, V. Shalaev, A. Boltasseva, and M. Ferrera, "Controlling hybrid nonlinearities in transparent conducting oxides via two-colour excitation," Nat. Commun. **8**, 15829 (2017).
44. M. Conforti and G. D. Valle, "Derivation of third-order nonlinear susceptibility of thin metal films as a delayed optical response," Phys. Rev. B **85**, 245423 (2012).
45. M. Scalora, J. Trull, D. de Ceglia, M. A. Vincenti, N. Akozbek, Z. Coppens, L. Rodriguez-Sune, and C. Cojocaru, "Electrodynamics of conductive oxides: intensity-dependent anisotropy, reconstruction of the effective dielectric constant, and harmonic generation," Phys. Rev. A **101**, 053828 (2020).
46. D. de Ceglia, M. Scalora, M. A. Vincenti, S. Campione, K. Kelley, E. L. Runnerstrom, J. P. Maria, G. A. Keeler, and T. S. Luk, "Viscoelastic optical nonlocality of low-loss epsilon-near-zero nanofilms," Sci. Rep. **8**, 9335 (2018).
47. M. Kauranen and A. V. Zayats, "Nonlinear plasmonics," Nat. Photonics **6**, 737–748 (2012).
48. R. del Coso and J. Solis, "Relation between nonlinear refractive index and third-order susceptibility in absorbing media," J. Opt. Soc. Am. B **21**, 640–644 (2004).
49. R. W. Boyd, Z. M. Shi, and I. De Leon, "The third-order nonlinear optical susceptibility of gold," Opt. Commun. **326**, 74–79 (2014).
50. D. D. Smith, Y. Yoon, R. W. Boyd, J. K. Campbell, L. A. Baker, R. M. Crooks, and M. George, "z-scan measurement of the nonlinear absorption of a thin gold film," J. Appl. Phys. **86**, 6200–6205 (1999).
51. K. P. Wang, J. Wang, J. T. Fan, M. Lotya, A. O'Neill, D. Fox, Y. Y. Feng, X. Y. Zhang, B. X. Jiang, Q. Z. Zhao, H. Z. Zhang, J. N. Coleman, L. Zhang, and W. J. Blau, "Ultrafast saturable absorption of two-dimensional MoS_2 nanosheets," ACS Nano **7**, 9260–9267 (2013).
52. S. Kumar, M. Anija, N. Kamaraju, K. S. Vasu, K. S. Subrahmanyam, A. K. Sood, and C. N. R. Rao, "Femtosecond carrier dynamics and saturable absorption in graphene suspensions," Appl. Phys. Lett. **95**, 191911 (2009).
53. A. Mayer and F. Keilmann, "Far-infrared nonlinear optics. II. $\chi^{(3)}$ contributions from the dynamics of free-carriers in semiconductors," Phys. Rev. B **33**, 6962–6968 (1986).